Coordinated control of grid-forming converters and hydro generators to enhance frequency quality of future power system

Electric Power Systems Research 212 (2022) 108456

Contents lists available at ScienceDirect

Electric Power Systems Research

journal homepage: www.elsevier.com/locate/epsr

Coordinated control of grid-forming converters and hydro generators to enhance frequency quality of future power system ☆

Anant Narula [a,*], Massimo Bongiorno [a], Mebtu Beza [a], Peiyuan Chen [a], Daniel Karlsson [b]

[a] Department of Electrical Engineering Chalmers University of Technology Gothenburg, Sweden
[b] Power System Analysis, Energy Advisory DNV Malmö, Sweden

ARTICLE INFO

Keywords:
Coordinated control
Frequency quality
Fast frequency response
Grid-forming converter
Synthetic inertia

ABSTRACT

The aim of this paper is to propose a coordinated control strategy between grid-forming converters equipped with energy storage, and hydro generators to facilitate frequency support from the converters in future power systems. In this way, it is possible to take advantage of the fast dynamic properties of the converter system, and at the same time minimize the energy storage requirements associated with the converter system. The proposed tuning criterion for the frequency controller of the grid-forming converter facilitates a natural coordination between the converter system and hydro generators. The effectiveness of the proposed control strategy is compared against the conventional droop-based approach available in the literature. Finally, the analytical findings are validated using detailed time-domain simulation model in PSCAD.

1. Introduction

In line with the initiatives undertaken to reduce greenhouse-gas emissions, the power system is witnessing a transition from fossil-fuel based generation to renewable energy sources (RES), which are typically connected to the grid through voltage-source converters (VSCs) [1]. However, the reduction of the rotating mass in the system brings in a number of challenges associated to low-inertia systems [1]. This includes the risk of high rate-of-change-of-frequency (RoCoF) leading to fast and potentially large frequency deviations, which may trigger undesirable events such as load-shedding and large-scale blackouts [2]. Hence, maintaining the grid frequency and RoCoF, which are the key indicators of frequency quality, within an acceptable range is essential for the stable operation of the power system [3].

Taking the case of the Nordic synchronous area, hydro generators which are the main providers of the frequency containment reserve (FCR), provide balancing actions following a momentary mismatch between generation and demand. However, with a reduction of the total system inertia in the future, the response time of the conventional FCR may not be sufficient to maintain the frequency nadir following a disturbance within the prescribed limit [4]. To account for this, grid-connected converter systems are expected to contribute towards system inertia and frequency support. Converter systems offer a great potential to provide frequency support at much faster timescales as compared to the conventional synchronous generator-based units. In particular, grid-forming converters facilitate the provision of important ancillary services, such as the inertial response, and black-start capability owing to its control structure [5]. Although the role of such converter systems in improving the frequency quality of the future RES-dominated power systems has been widely addressed in the literature [6–11], little effort has been put to reduce the VSC's energy storage requirements for performing such regulations. This is a crucial aspect especially for the converter systems with limited active-power injection capability, such as a static compensator (STATCOM) integrated with an energy storage (for e.g. a supercapacitor), participating in dynamic frequency support [12,13]. Some case studies presented in the literature suggest the use of adaptive control for grid-forming converters, aimed at reducing the needed energy storage [14]. However, online variation of the control parameters of the converter is typically not recommended by the system operators [15]. Keeping in mind that the future grid will still include conventional generation, a valuable alternative to minimize the converter's energy storage requirements is to coordinate the frequency support from synchronous generators with the one offered by converter systems. However, to the best of our knowledge, works on such coordination aspects are currently very limited and needs to be addressed further [16–18].

The aim of this paper is to propose a coordinated control strategy between grid-forming converters and hydro generators, in order to improve the frequency quality in the power systems with high penetration of RES, and at the same time reduce the energy storage requirements of the converter system. This is achieved by providing fast support

☆ Submitted to the 22nd Power Systems Computation Conference (PSCC 2022).

* Corresponding author.
E-mail addresses: anant.narula@chalmers.se (A. Narula), daniel.karlsson@dnv.com (D. Karlsson).

https://doi.org/10.1016/j.epsr.2022.108456
Received 3 October 2021; Received in revised form 16 April 2022; Accepted 2 July 2022
Available online 19 July 2022

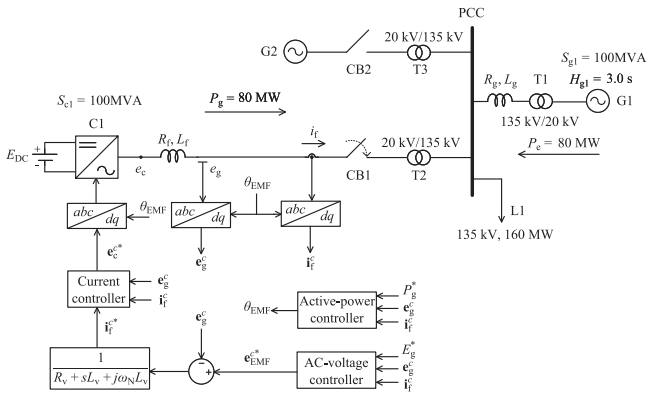

Fig. 1. Single-line diagram of investigated system together with main block-scheme of the implemented grid-forming converter control.

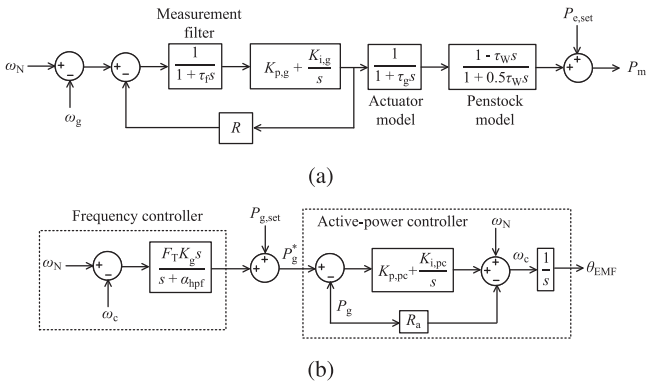

Fig. 2. Block-scheme of the (a) hydro governor (b) active-power controller of the grid-forming converter.

from the converter system in comparison to the hydro generators in the initial phase of the transient, thereby reducing the RoCoF and preventing large frequency deviation, and gradually reducing it, in order to allow the hydro generators to properly contribute to system's frequency regulation. Thanks to the proposed tuning criterion for the frequency controller of grid-forming converters, this action takes place naturally. The effectiveness of the proposed control strategy is validated in the well-known Kundur's four-machines/two-area system using detailed time-domain simulations in PSCAD.

2. Structure of grid-forming converter control and problem formulation

Several control strategies for the grid-forming converter can be found in the literature [19–21]. One common feature for the majority of the grid-forming converter control strategies is that the active-power controller provides grid-synchronization for the converter system. The virtual-admittance based control [20] is implemented here since it is found to be more robust against system variations as compared to other grid-forming converter control strategies [22]. In addition, it models the grid-forming converter as a controllable-voltage source behind an impedance which is one of the future requirements from the European Network of Transmission System Operators for Electricity (ENTSO-E) [5]. In the virtual-admittance based control, the outer active-power controller calculates the phase-angle of the virtual back-electromotive force (EMF) of the emulated virtual machine, while the ac-voltage controller regulates the voltage at the point-of-common-coupling (PCC), by calculating the magnitude of the virtual back-EMF. The virtual admittance, which represents the total admittance between the PCC-voltage and virtual back-EMF, calculates the reference values for the inner-current controller. Finally, the inner-current controller calculates the reference voltage for the modulation stage. For a fair comparison of various case studies in consideration, an ideal-voltage source at the DC side of the converter is assumed. Nevertheless, the impact of the frequency controller of the grid-forming converter on the VSC's energy storage requirements is discussed later.

Fig. 1 shows the investigated system together with the block-scheme of the implemented virtual-admittance based control. For the purpose of simplicity, a one-bus system is considered here. As shown in the figure, the system consists of a VSC 'C1' connected at the PCC through a transformer 'T2', and a filter reactor of resistance, R_f, and inductance, L_f. The voltage at the PCC and at the converter's terminal are denoted by e_g and e_c, respectively; i_f is the current flowing across the converter's filter. A constant active-power load 'L1' is connected at the PCC. The ac-grid is represented by a synchronous generator 'G1' connected at the PCC through a transformer 'T1', and a grid impedance of resistance, R_g, and inductance, L_g. For the case study presented in this section, the synchronous generator 'G2' is kept disconnected. The rating of the different system components, together with the operating point of the two generation units are shown in the figure. A well-established hydro governor model used for the Nordic 32 system is implemented for 'G1', see Fig. 2(a) [23].

For a proper reference tracking, a proportional–integral (PI) based active-power controller as the one proposed in [24] is used for the VSC, and is shown in Fig. 2(b). In order to provide the desired virtual inertia and damping, the proportional and integral gains ($K_{p,pc}$ & $K_{i,pc}$, respectively) are selected as [24]

$$K_{i,pc} = \frac{\omega_N}{2H_{conv}}; K_{p,pc} = \zeta\sqrt{\frac{2\omega_N X_v}{H_{conv}}}, \quad (1)$$

where ω_N is the rated angular frequency of the system (expressed in radians per second), H_{conv} represents the virtual-inertia constant (expressed in seconds), ζ is the damping ratio (in per-unit), and X_v is the virtual-inductive reactance (in per-unit) between the PCC-voltage and virtual back-EMF. In order to improve the dynamic performance of the active-power controller, an inner-feedback loop via an active-damping term, $R_a = \frac{K_{i,pc} X_v}{K_{p,pc}}$, is introduced [25].

In order to guarantee a stable operation of the power system, it is essential that the instantaneous frequency is kept within the prescribed limits. The limit for the frequency nadir is 49.0 Hz in the Nordic synchronous area [3]. With a reduction of the total system inertia in the future, it is expected that also RES (as well as dedicated converter systems) will contribute to the frequency support. For this, a frequency controller is added in cascade to the active-power controller as shown in Fig. 2(b). It is constituted by a high-pass filter having cut-off frequency, α_{hpf}, and gain K_g. The term F_T represents a triggering function that activates the frequency controller of the converter system only when the grid frequency crosses the threshold indicated by the Grid Code, and keeps it active until the system frequency has reached a new steady-state value. This kind of structure provides a frequency support from the converter system during transients only. As the main focus here is on the grid-connected converter systems with limited energy storage, the converter system is used here for FFR provision only. However, if the size of the VSC's energy storage is not a constraint, both FFR and FCR can be provided by simply removing the high-pass filter in the frequency controller, and selecting the proportional term based on the desired frequency-droop characteristic of the converter system.

By carefully selecting the parameters of the frequency controller (as described later in Section 3), a natural coordination between the grid-forming converter and hydro generator can be achieved, thereby reducing both peak power and energy storage requirements of the converter system. In order to demonstrate this, the response of the system following a step increase of 5 MW in the load (corresponding to

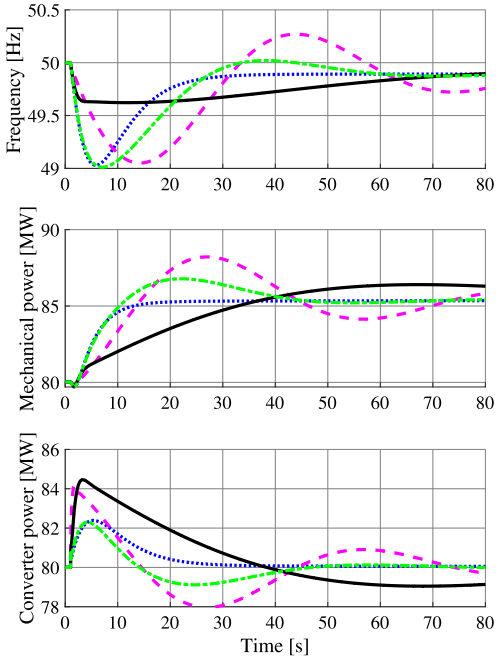

Fig. 3. Response of the system following a step increase in the load for four different settings of the frequency controller: *Case A* (solid black), *Case B* (dashed magenta), *Case C* (dotted blue), and *Case D* (dashed–dotted green).

approximately 3% of the total system load) is shown in Fig. 3 for the four case studies:

- *Case A*: High value of K_g, and low value of α_{hpf}: solid-black curves.
- *Case B*: High value of K_g, and high value of α_{hpf}: dashed-magenta curves.
- *Case C*: Low value of K_g, and low value of α_{hpf}: dotted-blue curves.
- *Case D*: Low value of K_g, and high value of α_{hpf}: dashed–dotted green curves.

It can be seen from the figure that *Case A* leads to an injection of high active power from the converter for a long duration. Hence, a relatively low frequency nadir is obtained as compared to the other cases. However, in this case the energy storage requirements of the converter system are significantly higher as compared to the other three cases, as the additional active-power injection is applied for a longer duration. This also results in a slower ramping of the mechanical power of the synchronous generator. Increasing α_{hpf} (*Case B*) leads to high active-power injection from the converter for a short duration. This reduces the energy storage requirements for the converter system significantly. Although the frequency nadir in this case is within the limit, the response of the system close to steady state is less damped as compared to all the other cases. In addition, the increase in the mechanical power of the synchronous generator is still slow, and can be improved further by reducing the value of K_g (*Cases C & D*). A faster increase in the mechanical power of the synchronous generator indicates a faster contribution from this unit to the system's frequency regulation. Reducing the value of K_g also leads to a reduction in the peak-power of the converter system, while still keeping the frequency nadir within the limit. A low value of α_{hpf} in *Case C* provides frequency support from the converter system for a longer duration as compared to both *Cases B & D*. This results in a very-well damped frequency response close to steady-state at the cost of higher energy storage requirements for the converter system.

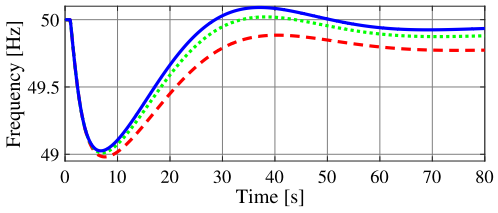

Fig. 4. Impact of the permanent droop of the governor on frequency response of the system following a step increase in the load for R = 0.08 pu (dashed red), 0.04 pu (dotted green), and 0.02 pu (solid blue).

The results from this study reveal that both converters and synchronous generators in the system must work in harmony, to provide the necessary frequency support to the system following an electrical disturbance. This not only improves the frequency response of the system, but also reduces the converter's additional active-power requirements for frequency support, both in terms of peak value and duration. For this, a proper tuning criteria for the two parameters, K_g and α_{hpf}, is proposed in the next section, which facilitates a natural coordination between the grid-forming converters and the synchronous generators in the system.

3. Modeling of system frequency dynamics and design of coordinated control

In this section, the frequency dynamics of a system comprising of only conventional synchronous generators are first modeled. The analysis performed using these models will serve as the basis for deriving the tuning criterion for the frequency controller of the grid-forming converter.

3.1. Frequency response model of system comprising of synchronous generators only

Once again the one-bus system shown in Fig. 1 is considered here; however, in this case the VSC is disconnected and the synchronous generator 'G2' having inertia constant, $H_{g2} = H_{g1} = 3$ s, and rated power, $S_{g2} = S_{g1} = 100$ MVA, is connected at the PCC. In order to understand the frequency dynamics of the system, the angular frequency, ω, and inertia constant, H_{coi}, corresponding to the center-of-inertia of the system are used for the analysis, and expressed as [26]

$$\omega = \frac{\omega_{g1}H_{g1}S_{g1} + \omega_{g2}H_{g2}S_{g2}}{H_{g1}S_{g1} + H_{g2}S_{g2}}; H_{coi} = \frac{H_{g1}S_{g1} + H_{g2}S_{g2}}{S_N}, \tag{2}$$

where ω_{g1} and ω_{g2} represent the angular frequency of 'G1' and 'G2', respectively. S_N denotes the rated power of the system, and is expressed as the sum of the rated power of the two generators. In order to keep the analysis simple, the same governor model (see Fig. 2(a)) is used for both generators. For obtaining a simplified expression for the transfer function, $G(s)$, from the input electrical disturbance, $\Delta P_e(s)$, to the change in the angular frequency of the system, $\Delta\omega(s)$, the time constant, τ_f, of the frequency-measurement filter in Fig. 2(a) is neglected, as it has a negligible impact on the time-scale of interest for frequency support. Furthermore, since the value of the permanent droop R is typically small, its impact during dynamic conditions can be neglected. In order to validate this claim, Fig. 4 shows the frequency response of the system, following a step increase of 5 MW in the load for three different values of R. It can be seen that varying R has a very little influence during the initial phase of the transient and on the frequency-nadir, but only affects the recovery of the system frequency and its steady-state value.

Hence, the transfer function, $G(s)$, can be expressed as

$$G(s) = \frac{\Delta\omega(s)}{\Delta P_e(s)} = \frac{-1}{2H_{coi}s + D(s)}, \tag{3}$$

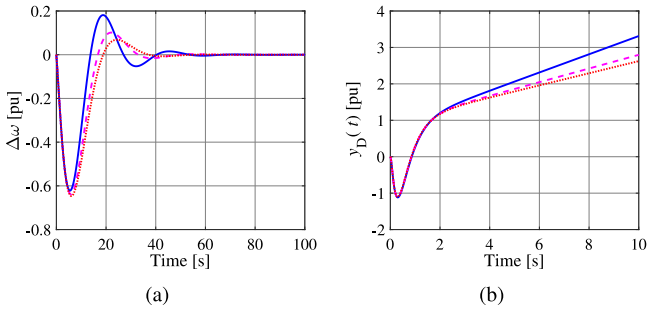

Fig. 5. Impact of the integral gain of the governor on (a) frequency response of the system following a unit-step disturbance (b) step response of $D(s)$; for $\tau_{r,g2}$ = 2X (dashed magenta), 3X (dotted red) of its initial value (solid blue).

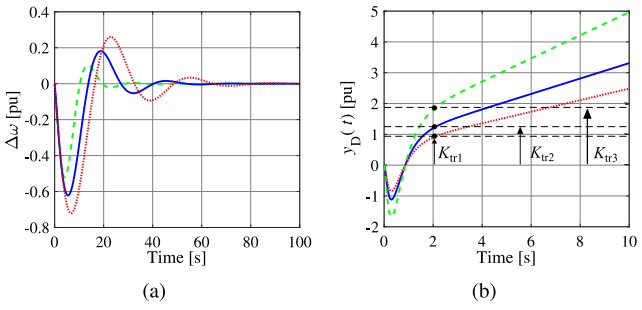

Fig. 6. Impact of the effective temporary-droop gain on (a) frequency response of the system following a unit-step disturbance (b) step response of $D(s)$; for r_{g2} = 0.5X (dashed green), 2X (dotted red) of its initial value (solid blue).

where

$$D(s) = \frac{(K_{p,g1}\frac{S_{g1}}{S_N} + K_{p,g2}\frac{S_{g2}}{S_N})s + (K_{i,g1}\frac{S_{g1}}{S_N} + K_{i,g2}\frac{S_{g2}}{S_N})}{s} \cdot \frac{(-\tau_w s + 1)}{(0.5\tau_w s + 1)}\frac{1}{(\tau_g s + 1)}. \quad (4)$$

The terms τ_w and τ_g represent the time constant of the penstock and actuator, respectively. The proportional gain (also referred to as the temporary-droop gain), $K_{p,g1}$ and $K_{p,g2}$, and integral gain, $K_{i,g1}$ and $K_{i,g2}$, of the two hydro governors are selected as [23]

$$K_{p,gn} = \frac{1}{r_{gn}};\ K_{i,gn} = \frac{1}{r_{gn}\tau_{r,gn}}; n \in \{1,2\}, \quad (5)$$

where r_{gn} and $\tau_{r,gn}$ denote the temporary droop and time constant of the nth hydro governor, respectively. The values of τ_w and τ_g depend upon the mechanical properties of the penstock and actuator, respectively, whereas the value of r_{gn} and $\tau_{r,gn}$ for hydro units are typically set in a similar range [23]. Some of the typical values of r_{gn}, $\tau_{r,gn}$, τ_w, and τ_g can be found in [23]. In this paper, r_{gn} = 0.8 pu, $\tau_{r,gn}$ = 5 s, τ_w = 1 s, and τ_g = 0.2 s are selected.

The impact of changing the system inertia, and the control parameters of one of the two governors, on the frequency response of the system is investigated next. This is used as a starting point to derive the parameters for the frequency controller of the grid-forming converter, when one of the conventional generators is replaced by a converter-interfaced generation unit.

3.1.1. Influence of integral gain on frequency response

The influence of the integral gain on the frequency response is investigated by varying the governor time-constant of 'G2', $\tau_{r,g2}$, and plotting the time-domain response, $\Delta\omega(t)$, using (3) and (4), for a unit-step disturbance. Fig. 5(a) shows the frequency response of the system for three different values of $\tau_{r,g2}$. It can be seen that varying $\tau_{r,g2}$ (or alternatively $K_{i,g2}$) has a very little influence on the frequency-nadir, and a significant impact on the recovery of the system frequency. The recovery is slowed down with a decrease in the value of $K_{i,g2}$. This can be understood by plotting the combined time-domain response of the two governors, $y_D(t)$, following a unit step in the frequency, using (4). As seen in Fig. 5(b), varying $K_{i,g2}$ has a negligible impact on the output of the two governors during the initial phase of the transient, thus on the frequency nadir following an electrical disturbance. The impact of reducing $K_{i,g2}$ is visible only during the later phase of the transient, in terms of a reduced integral action of the governor, leading to a slow recovery of the system frequency. It shall be noted that the initial negative phase in the output of the hydro governor is resulting from the non-minimal phase behavior of the penstock.

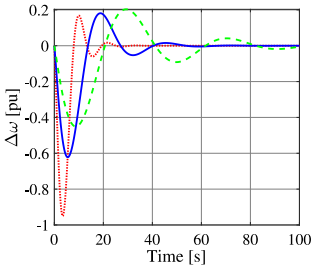

Fig. 7. Impact of the system inertia on the frequency response following a unit-step disturbance for H_{coi} = 2.0X (dashed green), 0.5X (dotted red) of its initial value (solid blue).

3.1.2. Influence of temporary-droop gain on frequency response

The influence of the temporary-droop gain on the frequency response is investigated by varying r_{g2}. Fig. 6(a) shows the frequency response of the system for three different values of r_{g2}. It can be seen that varying r_{g2} has a significant impact on the frequency nadir, speed of recovery, and damping. The frequency nadir improves when decreasing r_{g2}, or in other words increasing $K_{p,g2}$. In addition, both the speed of recovery and damping increase when decreasing r_{g2}. This can be explained by once again plotting $y_D(t)$. As it can be seen from (4) and Fig. 6(b), increasing $K_{p,g2}$ increases the effective temporary-droop gain, K_{tr}, defined as

$$K_{tr} = K_{p,g1}\frac{S_{g1}}{S_N} + K_{p,g2}\frac{S_{g2}}{S_N}. \quad (6)$$

This explains for the improvement in the frequency nadir and damping when increasing $K_{p,g2}$. In addition, it can be seen from (4) and (5), as well as Fig. 6(b) that the integral action of the governor also increases when decreasing r_{g2}, leading to a faster recovery of the system frequency.

3.1.3. Influence of system inertia on frequency response

Finally, the influence of the system inertia on the frequency response is investigated by varying the inertia constant, H_{coi}. Fig. 7 shows the frequency response of the system for three different values of H_{coi}. It can be seen that increasing the system inertia improves the frequency nadir; however, as expected, it leads to a slower recovery and a decreased damping.

3.2. Frequency response model of system comprising of a synchronous generator and a grid-forming converter

The synchronous generator 'G2' is now disconnected, while the grid-forming converter 'C1' is connected back at the PCC. In general, this can be seen as the case when a non-environmental friendly generating plant is replaced by RES. The hydro generators are still meant to be the

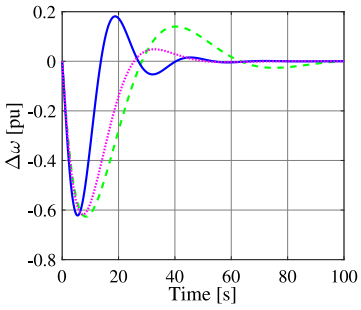

Fig. 8. Frequency response of the system following a unit-step disturbance for *Case A* (solid blue), *Case B* (dashed green), and *Case C* (dotted magenta).

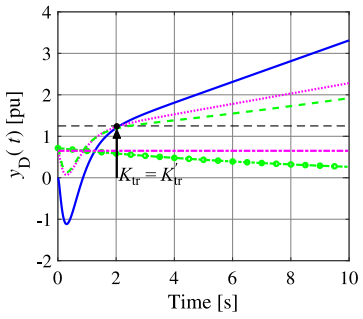

Fig. 9. Step response of $D(s)$ for *Case A* (solid blue), $D'(s)$ for *Case B* (dashed green) and *Case C* (dotted magenta), step response of the frequency controller of converter for *Case B* (green curve with round markers) and *Case C* (dashed–dotted magenta).

main providers of FCR. As the main focus of this paper is on the tuning criterion for the frequency controller of the grid-forming converter, the inertia constant, H_{coi}, is kept unchanged by emulating the same inertia as that of 'G2' in the converter (H_{conv} = 3 s). In analogy to the analysis carried out in the previous section, the transfer function, $G'(s)$, from the input electrical disturbance, $\Delta P_e(s)$, to the change in the angular frequency of the system, $\Delta\omega(s)$, can be written as

$$G'(s) = \frac{\Delta\omega(s)}{\Delta P_e(s)} = \frac{-1}{2H_{coi}s + D'(s)}, \tag{7}$$

where

$$D'(s) = \frac{(K_{p,g1}\frac{S_{g1}}{S_N})s + (K_{i,g1}\frac{S_{g1}}{S_N})}{s}\frac{(-\tau_w s+1)}{(0.5\tau_w s+1)}\frac{1}{(\tau_g s+1)} + F_T\frac{(K_g\frac{S_{c1}}{S_N})s}{(s+\alpha_{hpf})}. \tag{8}$$

From the analysis performed in the previous section, the frequency nadir is greatly influenced by the system inertia, and the effective temporary-droop gain. Since H_{coi} is kept unchanged, to obtain a similar or better performance in terms of the frequency nadir, the effective gain, K'_{tr}, should be

$$K'_{tr} = K_g\frac{S_{c1}}{S_N} + K_{p,g1}\frac{S_{g1}}{S_N} \geq K_{tr}. \tag{9}$$

Comparing (6) and (9), we can say that for this case, $K_g \geq K_{p,g2}\frac{S_{g2}}{S_{c1}}$. In addition, the removal of the frequency support from the converter system should not be faster than the increment in the support from the hydro generator, which is dictated by the integral gain of the hydro governor (discussed later in Section 4). For this, the value of α_{hpf} should be selected smaller than or equal to the integral gain of 'G1', i.e., $\alpha_{hpf} \leq K_{i,g1}\frac{S_{g1}}{S_N}$. The upper limit of K_g depends on the power rating of the converter and the capacity of the energy storage, whereas the lower limit of α_{hpf} depends on the capacity of the energy storage only.

Fig. 8 shows the frequency response of the system following a unit-step disturbance for the following three cases:

- *Case A*: Two synchronous generators in the system (base case): solid-blue curve.
- *Case B*: One synchronous generator and one grid-forming converter in the system with $K_g = K_{p,g2}$ and $\alpha_{hpf} = 0.5K_{i,g1}$: dashed-green curve.
- *Case C*: One synchronous generator and one grid-forming converter in the system with $K_g = K_{p,g2}$ and $\alpha_{hpf} = 0$. This is equivalent to the conventional droop-based frequency controller: dotted-magenta curve.

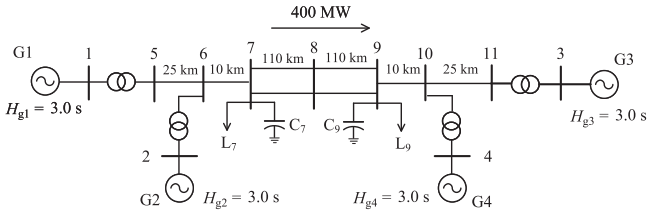

Fig. 10. Two-area system used to verify the proposed coordination between the converter-interfaced generation units and hydro generators in the system.

It can be seen from Fig. 8 that in *Case B* the frequency nadir is very close to that of the base case. However, both the speed of recovery and damping are reduced. These phenomena can be explained by plotting $y_D(t)$ for *Case A* and $y'_D(t)$ for *Case B*. It can be seen from Fig. 9 that $K_{tr} = K'_{tr}$, which explains for a similar frequency nadir in the two cases. It can also be seen from the dashed-green curve in Fig. 9 that the integral action is reduced in *Case B*, which explains for the slower recovery of the system frequency. Furthermore, it can be seen from the green curve with round markers in Fig. 9 that the frequency support from the converter decreases over time in *Case B*, leading to a reduced damping. A decrease in the value of α_{hpf} (*Case C*) will provide a better damping and an increase in the speed of recovery, as can be visualized from the dotted-magenta curve in Fig. 8. However, this is at the cost of an increase in the energy storage requirements of the converter system (dashed-magenta curve in Fig. 9).

The proposed tuning criterion for the frequency controller of grid-connected converter systems can be generalized as follows: in order to prevent a deterioration of the frequency nadir following a given electrical disturbance, the gain K_g of the high-pass filter should be at least equal to the effective temporary-droop gain of the synchronous generators being replaced. On the other hand, the cut-off frequency of the high-pass filter, α_{hpf}, should be at most equal to the effective integral gain of the remaining synchronous generators in the network. To keep an adequate safety margin, it is beneficial to take into account the loss of the largest FCR providing unit in the system, while making the calculations for K_g and α_{hpf}. This will be discussed further in the next section.

4. Simulation results

As a proof of concept, the proposed design for the frequency controller of grid-forming converter is tested in the well-known Kundur's four-machines/two-area system shown in Fig. 10, using detailed time-domain simulation in PSCAD. The rating of the different system components, and the operating point of the generators are kept the same as in the original model [26]. However, the inertia constant of all the four generators is selected as 3 s. The hydro-governor model shown in Fig. 2(a) is used for all the synchronous generators. The system

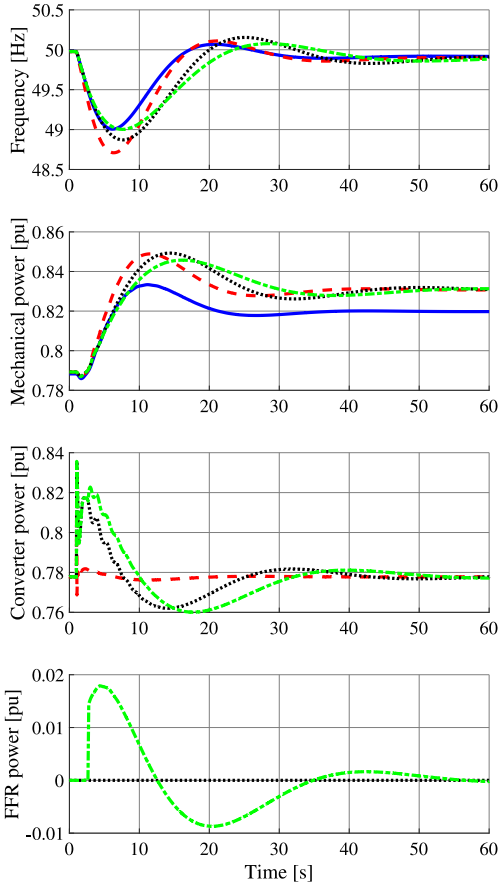

Fig. 11. Response of the system following the maximum dimensioning disturbance for four different cases: base-case (solid blue); converter providing neither inertia nor frequency support (dashed red), inertia support only (dotted black), inertia and frequency support in coordination with other synchronous generators (dashed–dotted green).

model with all four synchronous generators connected is selected as the base-case scenario for comparison purpose. It is found that when a step-increase of 113 MW (corresponding to approximately 4% of the total system load) is applied to the load connected at Bus 7, the frequency nadir of 49.0 Hz is obtained for the base-case scenario. Hence, this is selected as the maximum dimensioning disturbance in the system.

The synchronous generator 'G2' is now replaced by a grid-forming converter of similar ratings. Fig. 11 shows the frequency response of the system, mechanical power input of 'G1', active power output of the converter, and output of the converter's frequency controller (referred as FFR power in the figure), following the maximum dimensioning disturbance in the system. It can be seen from Fig. 11 that providing neither inertia nor frequency support from the converter leads to a deterioration of the frequency nadir below the acceptable limit. Furthermore, providing only inertia support from the converter improves the frequency-nadir; however, it is still below the acceptable limit. On the other hand, providing both inertia and frequency support from the converter makes the frequency nadir in this case equal to that obtained in the base-case scenario. Thanks to the proposed tuning criterion for α_{hpf}, the rate of change of the mechanical power input to the synchronous generator is not deteriorated by the presence of the converter. It can also be seen from the plot of the converter power (dashed–dotted green curve) that compared to the previous case (dotted-black curve), the converter provides additional active-power support for a longer duration. Therefore, the ramp-up time of the mechanical power input to the hydro generators is sufficient to keep the frequency nadir within permissible limits in this case. However, as expected from the theoretical analysis, the recovery of the system frequency in this case is slower than the base case. It shall be noted that in order to fulfill the requirements for providing FFR service, the frequency support from the converter starts when the system frequency drops below 49.5 Hz in this case, and not directly at the beginning of the transient [27]. In order to tune the frequency controller, the relations derived in the previous section are used here. Accordingly, the values of K_{g} and α_{hpf} are

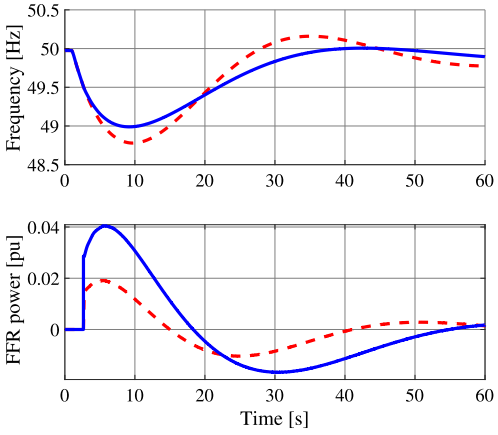

Fig. 12. Response of the system following the maximum dimensioning disturbance and loss of the largest FCR providing unit for two different settings of the frequency controller: according to (10) (dashed red), according to (11) (solid blue).

$$K_{\text{g}} = K_{\text{p,g2}}\frac{S_{\text{g2}}}{S_{\text{c1}}}; \alpha_{\text{hpf}} = \frac{K_{\text{i,g1}}S_{\text{g1}} + K_{\text{i,g3}}S_{\text{g3}} + K_{\text{i,g4}}S_{\text{g4}}}{S_{\text{N}}}. \tag{10}$$

As mentioned earlier, in order to keep an adequate safety margin, it is beneficial to take into account the loss of the largest FCR providing unit in the system, while making the calculations for K_{g} and α_{hpf}. The following case study is performed in support of this statement. To simulate the loss of a FCR providing unit following the maximum dimensioning disturbance in the system, the governor of the synchronous generator 'G1' is now disconnected, and the tuning for the frequency controller of grid-forming converter is kept unchanged. The frequency response of the system, and output of the converter's frequency controller for this case are shown by the dashed-red curves in Fig. 12. As expected, the frequency nadir in this case falls below 49.0 Hz. This is due to an injection of insufficient additional power from the converter following the disturbance. To avoid this, the tuning for the frequency controller of the grid-forming converter should be modified as

$$K_{\text{g}} \geq \frac{K_{\text{p,g1}}S_{\text{g1}} + K_{\text{p,g2}}S_{\text{g2}}}{S_{\text{c1}}}; \alpha_{\text{hpf}} \leq \frac{K_{\text{i,g3}}S_{\text{g3}} + K_{\text{i,g4}}S_{\text{g4}}}{S_{\text{N}}}. \tag{11}$$

The solid-blue curves in Fig. 12 show the frequency response, and output of the converter's frequency controller, for the minimum and maximum value of K_{g} and α_{hpf}, respectively, according to (11). As expected, the frequency-nadir in this case is at 49.0 Hz. This is due to an increase in the value of K_{g}, which results in an injection of higher active power from the converter in the beginning of the frequency support. It can also be seen from the plot of FFR power (solid-blue curve) that the converter now supports the system for a longer duration, due to a decrease in the value of α_{hpf}. This in turn provides a relatively more damped frequency response closer to steady state in this case.

In order to validate the effectiveness of the proposed tuning criteria (11) in other case scenarios as well, the governor of the synchronous generator 'G1' is re-connected and the maximum dimensioning disturbance is applied in the system. Fig. 13 shows the frequency response of the system with two different settings of the frequency controller. It can be seen from the solid-blue curve in Fig. 13 that with the tuning criteria for the frequency controller as in (11), the frequency

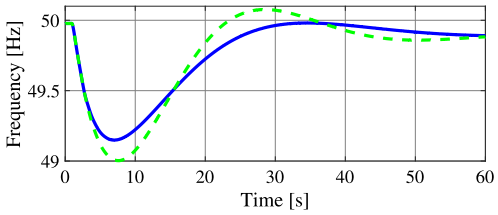

Fig. 13. Frequency response of the system following the maximum dimensioning disturbance for two different settings of the frequency controller: according to (10) (dashed green), according to (11) (solid blue).

response is improved both in terms of its minimum instantaneous value and damping. In addition, keeping an adequate safety margin while tuning the frequency controller of grid-forming converter also helps in dealing with the uncertainty of the grid topology, and connected FCR-providing units in the power system. The case studies presented in this section validate the effectiveness of the proposed tuning criterion for the frequency controller of the grid-forming converter.

5. Conclusion

A coordinated control strategy between the grid-forming converters and hydro generators is proposed in this paper to provide frequency support in RES-dominated power systems. It utilizes the fast dynamic properties of the converter system to keep the instantaneous frequency following an electrical disturbance within the prescribed limits, without deteriorating the performance of the remaining synchronous generators in the system. This not only improves the frequency response of the system, but also minimizes the energy storage requirements of the converter system. It is shown that with the proposed tuning criterion for the frequency controller of grid-forming converters, a natural coordination is achieved between the two types of generation units. Finally, the effectiveness of the proposed coordination is validated in the Kundur's four-machines/two-area system using detailed time-domain simulations in PSCAD.

CRediT authorship contribution statement

Anant Narula: Conceptualization, Methodology, Software, Validation, Formal analysis, Investigation, Writing – original draft, Writing – review & editing, Visualization. **Massimo Bongiorno:** Conceptualization, Methodology, Software, Writing – review & editing, Visualization, Resources, Project administration, Funding acquisition. **Mebtu Beza:** Conceptualization, Methodology, Software, Writing – review & editing, Visualization. **Peiyuan Chen:** Conceptualization, Methodology, Software, Writing – review & editing, Visualization. **Daniel Karlsson:** Conceptualization, Methodology, Software, Writing – review & editing, Visualization.

Declaration of competing interest

The authors declare that they have no known competing financial interests or personal relationships that could have appeared to influence the work reported in this paper.

References

[1] F. Milano, F. Dörfler, G. Hug, D.J. Hill, G. Verbič, 2018 Power Systems Computation Conference (PSCC), Foundations and Challenges of Low-Inertia Systems (Invited Paper), 2018, pp. 1–25.
[2] D. Obradović, M. Ghandhari, R. Eriksson, Assessment and design of frequency containment reserves with HVDC interconnections, in: 2018 North American Power Symposium (NAPS), 2018, pp. 1–6.
[3] Explanatory Document for the Nordic Synchronous Area Proposal for Frequency Quality Defining Parameters and the Frequency Quality Target Parameter, Tech. Rep., ENTSO-E, 2018.
[4] FCR-D Design of Requirements – Phase 2, Tech. Rep., ENTSO-E, 2019.
[5] High Penetration of Power Electronic Interfaced Power Sources and the Potential Contribution of Grid Forming Converters, Tech. Rep., ENTSO-E, 2020.
[6] W. Zhang, D. Remon, P. Rodriguez, Frequency support characteristics of grid-interactive power converters based on the synchronous power controller, IET Renew. Power Gener. 11 (4) (2017) 470–479.
[7] Q. Hong, M. Nedd, S. Norris, I. Abdulhadi, M. Karimi, V. Terzija, B. Marshall, K. Bell, C. Booth, Fast frequency response for effective frequency control in power systems with low inertia, J. Eng. 2019 (16) (2019) 1696–1702.
[8] C. Mosca, F. Arrigo, A. Mazza, E. Bompard, E. Carpaneto, G. Chicco, P. Cuccia, Mitigation of frequency stability issues in low inertia power systems using synchronous compensators and battery energy storage systems, IET Gener. Transm. Distrib. 13 (17) (2019) 3951–3959.
[9] P.V. Brogan, R.J. Best, D.J. Morrow, K. McKinley, M.L. Kubik, Effect of BESS response on frequency and RoCoF during underfrequency transients, IEEE Trans. Power Syst. 34 (1) (2019) 575–583.
[10] Y. Yoo, S. Jung, G. Jang, Dynamic inertia response support by energy storage system with renewable energy integration substation, J. Mod. Power Syst. Clean Energy 8 (2) (2020) 260–266.
[11] L. Meng, et al., Fast frequency response from energy storage systems—A review of grid standards, projects and technical issues, IEEE Trans. Smart Grid 11 (2) (2020) 1566–1581.
[12] E. Spahic, C.P. Susai Sakkanna Reddy, M. Pieschel, R. Alvarez, Multilevel STATCOM with power intensive energy storage for dynamic grid stability - frequency and voltage support, in: 2015 IEEE Electrical Power and Energy Conference (EPEC), 2015, pp. 73–80.
[13] M.P.S. Gryning, B. Berggren, L.H. Kocewiak, J.R. Svensson, Delivery of frequency support and black start services from wind power combined with battery energy storage, in: 19th Int'L Wind Integration Workshop, 2020, pp. 1–10.
[14] U. Markovic, N. Früh, P. Aristidou, G. Hug, Interval-based adaptive inertia and damping control of a virtual synchronous machine, in: 2019 IEEE Milan PowerTech, 2019, pp. 1–6.
[15] Minimum Specification Required for Provision of GB Grid Forming (GBGF) Capability (Formerly Virtual Synchronous Machine/VSM Capability), Tech. Rep., National Grid ESO, 2021.
[16] J. Björk, K.H. Johansson, F. Dörfler, Dynamic virtual power plant design for fast frequency reserves: Coordinating hydro and wind, in: IEEE Transactions on Control of Network Systems, 2022, http://dx.doi.org/10.1109/TCNS.2022.3181553.
[17] W. Zhong, J. Chen, M. Liu, M.A.A. Murad, F. Milano, Coordinated control of virtual power plants to improve power system short-term dynamics, Energies 14 (4) (2021) 1182.
[18] V. Haberle, M.W. Fisher, E. Prieto Araujo, F. Dorfler, Control design of dynamic virtual power plants: An adaptive divide-and-conquer approach, IEEE Trans. Power Syst. http://dx.doi.org/10.1109/TPWRS.2021.3139775.
[19] L. Zhang, L. Harnefors, H. Nee, Power-synchronization control of grid-connected voltage-source converters, IEEE Trans. Power Syst. 25 (2) (2010) 809–820.
[20] P. Rodriguez, I. Candela, C. Citro, J. Rocabert, A. Luna, Control of grid-connected power converters based on a virtual admittance control loop, in: 2013 15th European Conference on Power Electronics and Applications (EPE), 2013, pp. 1–10.
[21] T. Qoria, F. Gruson, F. Colas, X. Guillaud, M. Debry, T. Prevost, Tuning of cascaded controllers for robust grid-forming voltage source converter, in: 2018 Power Systems Computation Conference (PSCC), 2018, pp. 1–7.
[22] A. Narula, M. Bongiorno, M. Beza, Comparison of grid-forming converter control strategies, in: 2021 IEEE Energy Conversion Congress and Exposition (ECCE), 2021, pp. 361–368.
[23] Long Term Dynamics – Phase II – Final Report, Tech. Rep., CIGRE, 1995.
[24] M.G. Taul, X. Wang, P. Davari, F. Blaabjerg, Current limiting control with enhanced dynamics of grid-forming converters during fault conditions, IEEE J. Emerg. Sel. Top. Power Electron. 8 (2) (2020) 1062–1073.
[25] A. Narula, M. Bongiorno, M. Beza, P. Chen, Tuning and evaluation of grid-forming converters for grid-support, in: 2021 23rd European Conference on Power Electronics and Applications, 2021, pp. 1–10.
[26] P. Kundur, Power System Stability and Control, McGrawHill, New York, 1994.
[27] FFR Design of Requirements – External Document, Tech. Rep., ENTSO-E, 2020.